

Energy dependence of elastic scattering and one-nucleon transfer reactions induced by ^{16}O on ^{208}Pb . II

C. Olmer,* M. Mermaz,† M. Buenerd,‡ C. K. Gelbke,§ D. L. Hendrie, J. Mahoney, and D. K. Scott
Lawrence Berkeley Laboratory, University of California, Berkeley, California 94720

M. H. Macfarlane and S. C. Pieper
Argonne National Laboratory, Argonne, Illinois 60439
(Received 3 January 1978)

The elastic scattering and single-nucleon stripping reactions induced by 312.6 MeV ^{16}O on ^{208}Pb are investigated and compared with data at lower incident energies. Distorted-wave Born-approximation analyses account rather well for the relative final-state yields at each energy, but fail to reproduce the absolute energy dependence of the observed transfer cross sections.

[NUCLEAR REACTIONS $^{208}\text{Pb}(^{16}\text{O}, ^{16}\text{O})$, $^{208}\text{Pb}(^{16}\text{O}, ^{15}\text{N})$, $^{208}\text{Pb}(^{16}\text{O}, ^{15}\text{O})$, $E_L = 312.6$ MeV; measured $\sigma(\theta)$; optical model and DWBA analyses; energy dependence of DWBA.]

I. INTRODUCTION

Studies of single-nucleon transfer reactions induced by light and heavy ions have been extremely useful in examining single-particle aspects of nuclear levels. In most of these studies, a direct one-step transfer model is assumed, the model predictions are calculated and, finally, the resulting transition strengths are compared with the experimental data. Although this procedure is often quite successful, a number of problems arise. The first difficulty concerns the extent to which the one-step distorted-wave Born approximation (DWBA) is a useful description of the transfer process. A second problem arises if the model calculations are very sensitive to aspects of the internal structure of the nuclear states (for example, the radial form of the single-nucleon overlap functions), for which neither experimental information nor adequate theoretical models are available. However, as is demonstrated in the preceding¹ and present papers, when the analyses are performed for a particular transfer reaction over a wide range of incident energy, rather than at a single isolated energy, the validity of the reaction model can be tested more stringently since the calculated energy dependence of the transfer cross sections is relatively insensitive to uncertainties in the treatment of the overlap functions.

In the present work, we have investigated the $^{208}\text{Pb}(^{16}\text{O}, ^{15}\text{N})^{209}\text{Bi}$ and $^{208}\text{Pb}(^{16}\text{O}, ^{15}\text{O})^{209}\text{Pb}$ reactions at an incident energy of 312.6 MeV. Initial results of a DWBA analysis of the proton-transfer data have been reported elsewhere.² The projectile and target are closed-shell nuclei for both neutron- and proton-transfer reactions,

and the low-lying levels in the residual nuclei are known to have large single-particle or single-hole components. As a result, a comparison of DWBA predictions for transitions to these states to data at 312.6 MeV and at lower incident energies^{1,3-5} (thereby spanning the region from below the Coulomb barrier to more than 200 MeV above the Coulomb barrier) provides a sensitive test of the reaction model.

Further interest in these studies results from our earlier measurements⁶⁻⁸ of light- and heavy-ion emission from the interaction of 315 MeV ^{16}O with various heavy targets, including ^{208}Pb . In that work, it was shown that data obtained at an incident energy of 315 MeV bear a remarkable resemblance, both qualitatively and quantitatively, to those measured in projectile fragmentation studies at an incident energy of 33.6 GeV. The incident energy of 20 MeV/A, close to the average Fermi energy, was found to characterize a transition between low-energy quasielastic and high-energy fragmentation processes. Experimental studies of the energy dependence of simple processes, such as elastic scattering and single-nucleon transfer, through this transition region, are important steps towards a unified treatment of low- and high-energy phenomena.

II. EXPERIMENTAL METHODS

The $^{208}\text{Pb}(^{16}\text{O}, ^{15}\text{N})^{209}\text{Bi}$ and $^{208}\text{Pb}(^{16}\text{O}, ^{15}\text{O})^{209}\text{Pb}$ reactions, as well as the elastic scattering of ^{16}O on ^{208}Pb were studied at the Lawrence Berkeley Laboratory 88-inch cyclotron using an incident beam of 312.6 MeV $^{16}\text{O}^{6+}$ with an intensity on the target of 10–100 nA. In the early stages of these measurements, our main interest was in transfer

processes populating the continuum. Consequently, thick targets ($1-3 \text{ mg/cm}^2$, evaporated, self-supporting ^{208}Pb) were employed and the observed energy resolution was insufficient to distinguish transitions to the various low-lying levels in ^{209}Bi and ^{209}Pb . Later experiments were performed with a thinner target ($84 \mu\text{g/cm}^2$ ^{208}Pb evaporated onto a $15 \mu\text{g/cm}^2$ carbon backing), thereby permitting significantly better energy resolution (typically, 300 keV or $\Delta E/E \sim 0.1\%$).

The reaction products were detected using a quadrupole-sextupole-dipole (QSD) magnetic spectrometer and focal plane detection system. The focal plane detector used in the initial experiments has been described earlier.^{9,10} In the later experiments, the detector was modified^{11,12} to permit the measurement of additional horizontal and vertical position and dE/dx signals.

Differential cross sections were determined using the measured target thickness and integrated beam current. Dead time and target deterioration effects were monitored throughout the experiment. A small correction was applied to the absolute cross section normalization in order to bring the forward angle elastic scattering data into agree-

ment with Rutherford scattering cross sections. Corrections were also made to the elastic scattering cross sections for the finite entrance aperture of the spectrometer. These corrections were significant (2–12%) only for the most forward angle elastic scattering data ($\theta_{c.m.} < 15^\circ$), and did not seriously affect (<2%) the backward angle elastic scattering data ($\theta_{c.m.} > 15^\circ$). This correction was not applied to the transfer data, since the effect is estimated to be insignificant. The absolute cross section normalization is estimated to be accurate to $\pm 10\%$. Reaction products from light target contaminants (in particular, carbon and oxygen) were kinematically excluded from the measurements reported here. Transfer data obtained at angles forward of $\theta_{lab} = 8^\circ$ were not sufficiently separated from reactions on target contaminants, and were not included in the final analyses.

III. DISCUSSION OF THE ENERGY SPECTRA

Energy spectra for the $^{208}\text{Pb}(^{16}\text{O}, ^{15}\text{N})^{209}\text{Bi}$ reaction at four incident energies, each measured near the angle of maximum transfer probability, are displayed in Fig. 1. The spectrum shown in

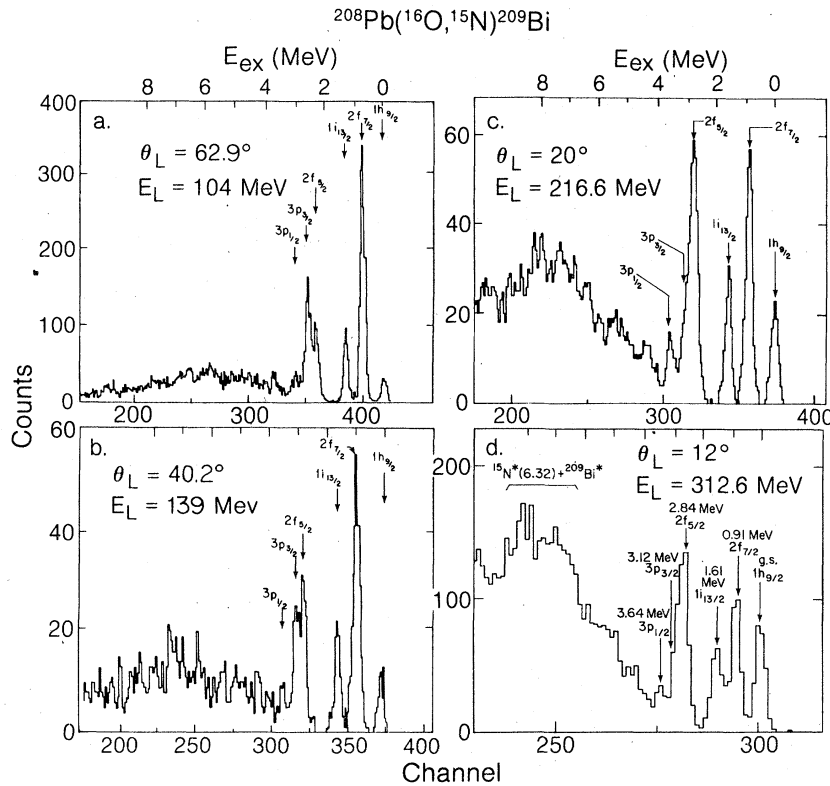


FIG. 1. Energy spectra obtained for the $^{208}\text{Pb}(^{16}\text{O}, ^{15}\text{N})^{209}\text{Bi}$ reaction at incident energies of 104, 138.5, 216.6, and 312.6 MeV. Transitions to known proton single-particle states are labeled according to their shell-model orbitals.

part (d) of the figure was obtained in the present work; the data in parts (a)-(c) were measured in earlier studies^{1,4} of this reaction at lower bombarding energies. Prominent in all these energy spectra are transitions to well known single-particle states in ²⁰⁹Bi, and these are labeled by their shell-model orbitals.

As has been previously observed for the data in parts (a)-(c) and for data measured for similar transfer reactions (see, for example, Ref. 13), the spectra exhibit a characteristic dependence on the single-particle angular momentum j . At low bombarding energies, spin-flip transitions are enhanced, i.e., a proton removed from a $j = l - \frac{1}{2} \equiv j_{\zeta}$ orbital, as in ¹⁶O, is preferentially transferred to a $j = l + \frac{1}{2} \equiv j_{\nu}$ orbital in the residual nucleus. Examples of this phenomenon are the intense yields to the $f_{7/2}$, rather than $f_{5/2}$, and $p_{3/2}$, rather than $p_{1/2}$, levels. A qualitative interpretation of this observation was presented in Ref. 13. At an incident energy of 312.6 MeV, however, a complete reversal of the j dependence is observed, and non-spin-flip transitions predominate; i.e., j_{ζ} rather than j_{ν} states in the residual nucleus are preferentially populated.

This reversal of the j dependence is accurately reproduced by DWBA calculations, as will be demonstrated in Sec. V. Further insight into the source of this phenomenon can be obtained by considering a semiclassical model of the transfer process.^{14,15} In this formulation, the transfer probability for the direct transfer of a nucleon (or cluster of nucleons) from an initial state specified by orbital and magnetic quantum numbers (l_1, λ_1) to a final state specified by (l_2, λ_2) is given by

$$P(\lambda_2, \lambda_1) \propto [Y_{l_1 \lambda_1}(\pi/2, 0) Y_{l_2 \lambda_2}(\pi/2, 0)]^2 \times \exp \left[- \left[\left(\frac{R \Delta k}{\sigma_1} \right)^2 - \left(\frac{\Delta L}{\sigma_2} \right)^2 \right] \right], \quad (1)$$

where

$$\Delta k = k_0 - \frac{\lambda_1}{R_1} - \frac{\lambda_2}{R_2}, \quad (2)$$

$$\Delta L = \lambda_2 - \lambda_1 + \frac{1}{2} k_0 (R_1 - R_2) + Q_{\text{eff}} \frac{R}{\hbar v}, \quad (3)$$

and

$$Q_{\text{eff}} = Q - (Z_1^f Z_2^f - Z_1^i Z_2^i) \frac{e^2}{R}. \quad (4)$$

In these equations, $k_0 = \Delta m v / \hbar$, $R = R_1 + R_2$, Δm is the mass of the transferred nucleon or cluster of nucleons, $v = [2(E_{CM} - E_{CB})/\mu]^{1/2}$ is the relative velocity in the region of transfer, R_1 and R_2 are the radii of the projectile and target nuclei, respectively, and σ_1 and σ_2 measure the widths of the Δk and ΔL distributions and are of similar magnitude.^{14,15}

For a large transfer probability, $\Delta k \approx 0$ and $\Delta L \approx 0$, corresponding to the conservation of linear and angular momenta of the transferred particle.

As an example, we consider the ²⁰⁸Pb(¹⁶O, ¹⁵N)-²⁰⁹Bi reaction populating the $2f_{7/2}$ and $2f_{5/2}$ levels in ²⁰⁹Bi at 0.90 and 2.84 MeV, respectively, since suitable experimental data are available for this particular spin-orbit pair over the entire range of incident energies discussed here. For these reactions, the values of l_1/R_1 and l_2/R_2 are similar in magnitude and the value of Q_{eff} is negative for both reactions. For low incident energies, the transfer velocity is much smaller than the orbital velocities, and the second and third terms of Eq. (2) must nearly cancel in order that $\Delta k \approx 0$. This requirement also results from Eq. (3), since at low velocities the magnitude of the negative Q_{eff} term is sufficiently large that $\lambda_1 = -l_1$ and $\lambda_2 = +l_2$ result in the minimum value of $|\Delta L|$. The manifestation of this condition (under the assumption that the spin orientation of the transferred nucleon does not change) corresponds to the j dependence observed at low bombarding energies, i.e., spin-flip transitions are enhanced. At very high bombarding energies, v becomes much larger than the orbital velocities. Inspection of Eq. (2) then indicates that $\lambda_1 = +l_1$ and $\lambda_2 = +l_2$ are required in order to minimize the magnitude of Δk . Similar conclusions also result from Eq. (3), in which the Q_{eff} term is now negligible and the remaining negative k_0 term is sufficiently small that, in order for $\Delta L \approx 0$, λ_1 and λ_2 must be of the same sign. These conditions result in a prediction that non-spin-flip transitions are preferred, as in the case at 312.6 MeV. At intermediate energies, a simple inspection of Eqs. (2) and (3) is not sufficient to determine the model predictions, and detailed calculations of Eq. (1), considering all possible magnetic substates and including the angular momentum coupling terms, are necessary for a prediction of the relative strengths of j_{ζ} and j_{ν} states. Such calculations show that this semiclassical model predicts a too rapid evolution from spin-flip to non-spin-flip dominance.

Energy spectra for the ²⁰⁸Pb(¹⁶O, ¹⁵O)²⁰⁹Pb reaction at 139 and 312.6 MeV, each measured near the angle of maximum transfer probability, are shown in Fig. 2. The lower-energy data were obtained in earlier studies⁵ of this reaction. As in the proton-transfer spectra, several known single-particle states in the residual nucleus are preferentially populated. Also evident in the 312.6 MeV spectrum is a candidate for a $j_{15/2}$ fragment state, which was observed at the same excitation energy but only weakly populated, at lower in-

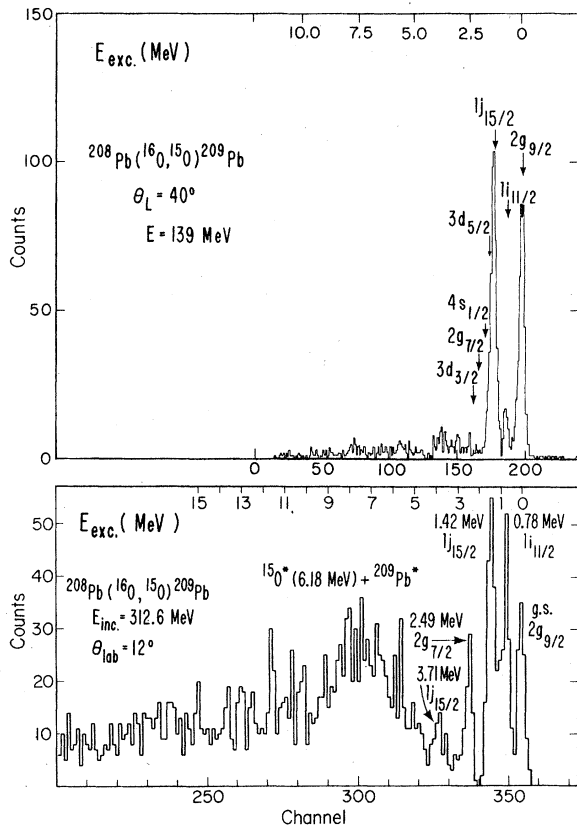


FIG. 2. Energy spectra obtained for the $^{208}\text{Pb}(^{16}\text{O}, ^{15}\text{O})^{209}\text{Pb}$ reaction at incident energies of 139 and 312.6 MeV. Transitions to known neutron single-particle states are labeled according to their shell-model orbitals.

incident energies.⁵ In the neutron-transfer spectra, the observed j dependence is somewhat different from that seen in the proton-transfer case. Transitions to j_z rather than j_z states are strongly enhanced at 139 MeV and this preference is still apparent, although much weaker, at 312.6 MeV, in contrast to the observation of a reversal of the j dependence for the proton-transfer reaction.

Application of the semiclassical model to the neutron-transfer reaction indeed indicates that the incident energy at which reversal of the j dependence is predicted is significantly higher than was predicted for the proton-transfer reaction. This result follows from inspection of Eq. (4), since the value of Q_{eff} is 12 MeV more negative for neutron transfer than for proton transfer. As a result, the Q_{eff} term is very large at low and intermediate bombarding energies and the largest transition amplitude occurs for $\lambda_1 = +l_1$ and $\lambda_2 = -l_2$. The Δk term must be considered for calculations at energies above 150 MeV, and at sufficiently high incident energies, where the Q_{eff} term is negligible, the considerations applied to

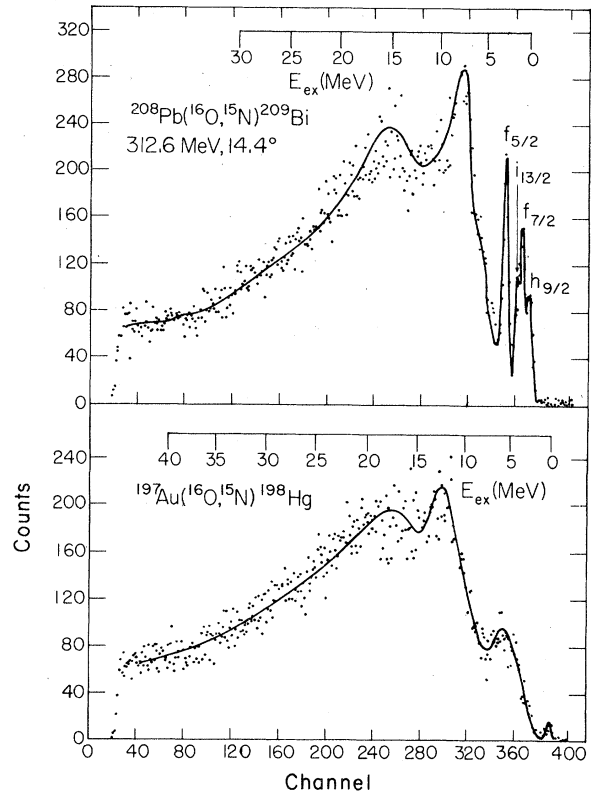


FIG. 3. Energy spectra measured at 14.4° for the $(^{16}\text{O}, ^{15}\text{N})$ reaction induced by 312.6 MeV ^{16}O on targets of ^{208}Pb and ^{197}Au .

the proton-transfer reaction may again be used. Thus a reversal of the j dependence would be indicated. However, as in the proton-transfer analysis, the predicted energy at which the reversal occurs is smaller than indicated by the data.

An additional feature in the proton- and neutron-transfer data which appears to have a strong dependence on incident energy is the yield to a broad structure centered at about 8 MeV in excitation. At the lowest energies [Figs. 1(a), 1(b), and 2(a)], this structure is barely visible and, as the incident energy is increased, its strength increases relative to that of transitions to the known single-particle states. The fact that this peak appears to be constant in excitation energy over a wide range of bombarding energy indicates that it is not the result of kinematic factors favoring the population of different final states with an optimum Q value, but rather reflects an increasing cross section for a definite excitation energy region.

This broad structure in the ^{209}Pb and ^{209}Bi spectra is again shown in Figs. 3 and 4, in which a larger portion of the excitation energy range is displayed for data obtained with thick targets ($1-3 \text{ mg/cm}^2$). The peak near 8 MeV in excitation

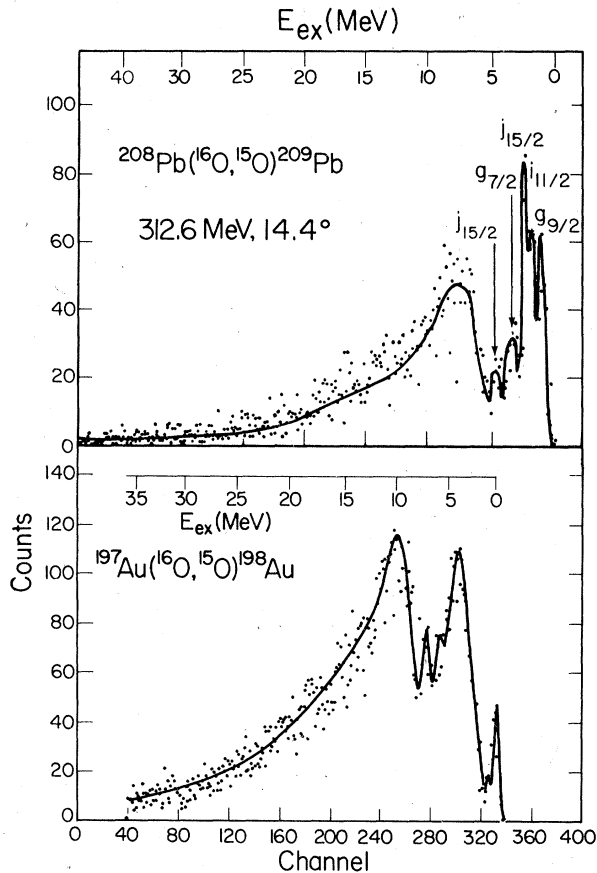


FIG. 4. Energy spectra measured at 14.4° for the $(^{16}\text{O}, ^{15}\text{O})$ reaction induced by $312.6\text{ MeV } ^{16}\text{O}$ on targets of ^{208}Pb and ^{197}Au .

is observed to be superimposed on a smooth background. Also shown in the figures are energy spectra for the $(^{16}\text{O}, ^{15}\text{N})$ and $(^{16}\text{O}, ^{15}\text{O})$ reactions on ^{197}Au , and the relatively intense excitation of several wide structures is apparent.

One possible source of these broad structures is single-nucleon transfer from one of the more deeply bound orbitals in ^{16}O (most probably the $p_{3/2}$ orbital) which would leave ^{15}N or ^{15}O in an excited state (6.32 or 6.18 MeV, respectively). The subsequent in-flight γ -ray decay of the reaction product would then give rise to a Doppler-broadened peak in the spectrum. In order to investigate this possibility, both proton- and neutron-transfer reactions were performed on ^{208}Pb and ^{197}Au targets using a 250 MeV incident ^{14}N beam (17.9 MeV/A incident energy as compared to 19.5 MeV/A for the ^{16}O beam). Since ^{13}N has no particle-stable excited states, significant differences between the $(^{16}\text{O}, ^{15}\text{O})$ and $(^{14}\text{N}, ^{13}\text{N})$ spectra could indicate that the ^{16}O -induced transfer data contain peaks originating from the excitation of ^{15}N and ^{15}O , together with the excitation of the

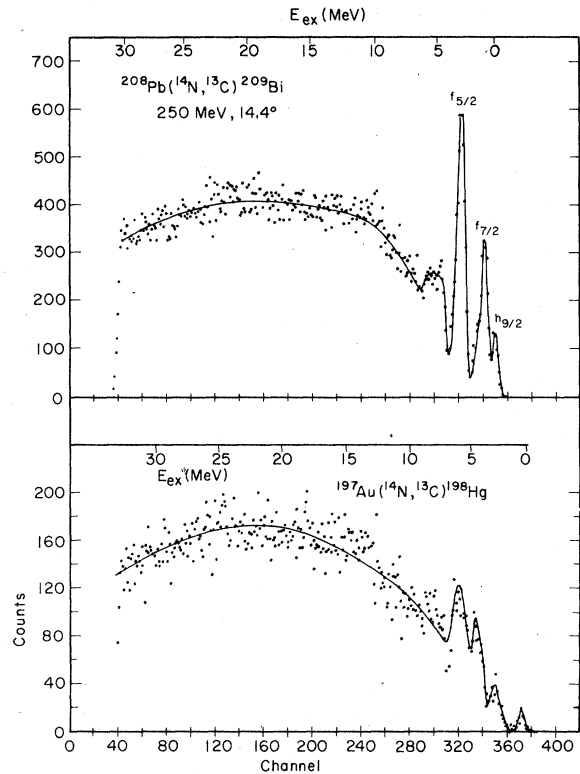


FIG. 5. Energy spectra measured at 14.4° for the $(^{14}\text{N}, ^{13}\text{C})$ reaction induced by 250 MeV ^{14}N on targets of ^{208}Pb and ^{197}Au .

heavier residual nuclei.

Energy spectra for the ^{14}N -induced proton- and neutron-transfer data are shown in Figs. 5 and 6. Similarities between the ^{16}O - and ^{14}N -induced neutron-transfer spectra displayed in Figs. 4 and 6 are evident. In particular, the intense population of several single-particle states in ^{209}Pb , including the suspected $j_{15/2}$ fragment, is visible in these spectra, and two broad structures, centered near 0 and 4 MeV in excitation, are observed in spectra for both the $(^{16}\text{O}, ^{15}\text{O})$ and $(^{14}\text{N}, ^{13}\text{N})$ reactions on ^{197}Au . In fact, the only significant difference between these data is that the peaks that appear near 7.5 MeV in excitation in the $^{208}\text{Pb}(^{16}\text{O}, ^{15}\text{O})^{209}\text{Pb}$ spectrum and near 10 MeV in the $^{197}\text{Au}(^{16}\text{O}, ^{15}\text{O})^{198}\text{Au}$ spectrum are absent in the corresponding $(^{14}\text{N}, ^{13}\text{N})$ spectra. This observation is consistent with the identification of the broad peaks in the $(^{16}\text{O}, ^{15}\text{O})$ spectra as the population of the excited state of ^{15}O (6.18 MeV) and one or more states in the heavy residual nucleus (approximately 1 and 4 MeV for the ^{209}Pb and ^{198}Au spectra, respectively). It will be demonstrated in Sec. V that a DWBA analysis confirms this identification.

A comparison of the ^{16}O and ^{14}N -induced proton-

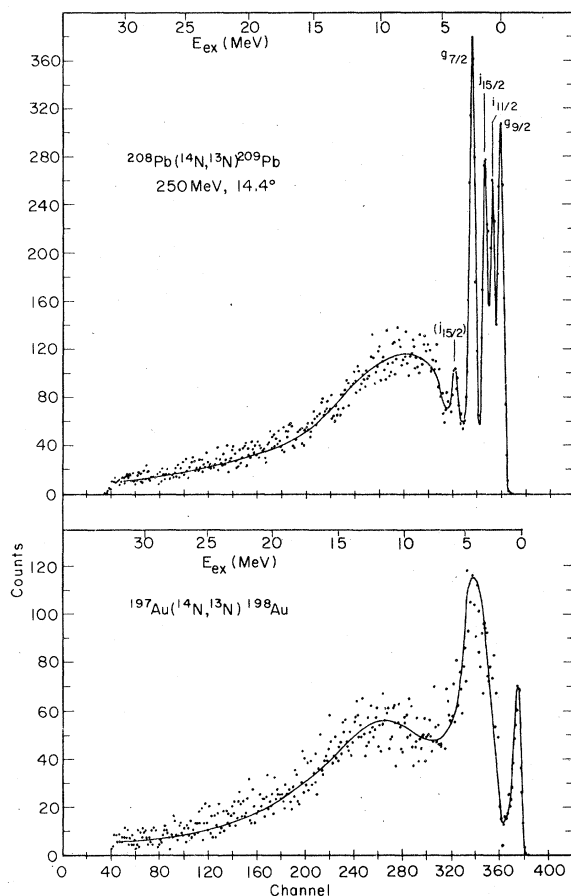


FIG. 6. Energy spectra measured at 14.4° for the $(^{14}\text{N}, ^{13}\text{N})$ reaction induced by 250 MeV ^{14}N on targets of ^{208}Pb and ^{197}Au .

transfer spectra shown in Figs. 3 and 5 also indicates the plausibility of this mechanism. The intense structure located near 8 (12) MeV in excitation for the $(^{16}\text{O}, ^{15}\text{N})$ reaction on ^{208}Pb (^{197}Au) is not apparent in the corresponding $(^{14}\text{N}, ^{13}\text{C})$ spectra, whereas other features in the spectra are similar. For example, the reversal of the low-energy j dependence, as exemplified by the stronger population at higher energy of the $f_{5/2}$ rather than $f_{7/2}$ state in ^{209}Bi , is observed for both the $(^{16}\text{O}, ^{15}\text{N})$ and $(^{14}\text{N}, ^{13}\text{C})$ reactions on ^{208}Pb .

The origin of the remaining structures in Figs. 3–6 is not well understood. The observed energies of many of these broad peaks correspond closely to known giant-resonance states seen, for example, in inelastic electron, proton, ^3He and α particle scattering.^{16–19} Recent $^{197}\text{Au}(p, p')$ ^{197}Au studies¹⁶ indicate a resonance near 4 MeV in excitation [full width at half maximum (FWHM) ~ 2 MeV] and a wider resonance near 12 MeV in excitation (FWHM ~ 4 MeV), in addition to the usual ground-state transition. These centroid-energies

(and, to a degree, the corresponding widths) are in remarkable correspondence with the structures appearing in the $^{197}\text{Au}(^{14}\text{N}, ^{13}\text{N})^{198}\text{Au}$ spectrum shown in Fig. 6. The excitation of giant-resonance states in the inelastic scattering of heavy ions by massive targets has not been extensively studied; however, recent experiments²⁰ have observed such processes in the inelastic scattering of 139 MeV ^{16}O ions by ^{197}Au . (In Ref. 20, the energy spectrum between 5 and 20 MeV in excitation was displayed. Two peaks, located near 6 and 12 MeV, are visible and the former, quite intense structure is probably the result of projectile excitation.) Unfortunately, the ^{16}O and ^{14}N inelastic scattering energy spectra obtained in the present work are not sufficient for a convincing identification of the structures observed in the transfer data as transitions to giant-resonance states.

Detailed inelastic scattering measurements are necessary since alternative explanations of the structures seen in the transfer spectra are conceivable: (i) The peak located near 4 MeV in excitation in the neutron-transfer spectra on ^{197}Au may reflect unresolved transitions to many discrete low-lying levels in ^{198}Au ; (ii) since several wide peaks appear in the spectrum rather than a single structure, it is conceivable that states in two major shells, both below and above the $Z = 82$, $N = 126$ closure, are being populated. Indeed, the energy gap between the closed-shell and high-spin states involving excitations into the higher shell is 4–5 MeV, and is in general agreement with the energy spacing between the peaks near 0 and 4 MeV in the ^{198}Au spectrum: (iii) the wide structure located at high excitation in all the spectra under consideration could result from the initial excitation of the projectile (for example, in the Coulomb field of the target) and its subsequent decay by proton or neutron emission. Thus, for example, the threshold for the neutron-fragmentation channel in the $^{197}\text{Au}(^{14}\text{N}, ^{13}\text{N})^{198}\text{Au}$ reaction would occur at 6.5 MeV in excitation and indeed, this energy seems to characterize the onset of the large continuum peak. Earlier studies²¹ of the interaction of 315 MeV ^{16}O with ^{208}Pb indicated that the position of the continuum peak in the energy spectra for elements from lithium to nitrogen generally could be reproduced with a simple fragmentation model.

IV. ELASTIC SCATTERING AND OPTICAL MODEL ANALYSES

The $^{16}\text{O} + ^{208}\text{Pb}$ elastic scattering angular distribution measured at an incident energy of 312.6 MeV is displayed²² in Fig. 7. Several optical-model descriptions of these data have been in-

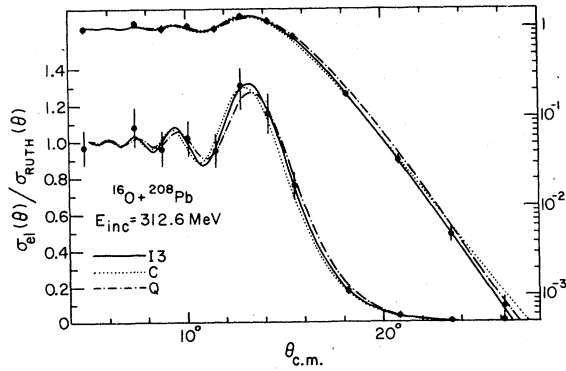


FIG. 7. Elastic-scattering angular distributions for 312.6 MeV ^{16}O on ^{208}Pb . The curves are optical-model fits using the parameters listed in Table I and discussed in the text.

investigated using the program PTOLEMY.²³ The resulting fits to the elastic scattering data will be discussed in this section; a discussion of the DWBA transfer calculations using these potentials will be presented in Sec. V.

Several sets of energy-dependent and energy-independent Woods-Saxon optical potentials which fit the elastic scattering data between 104 and 216.6 MeV have been derived.¹ The optical potential Q was obtained¹ from an 11-parameter global fit to the low-energy data ($E_{\text{lab}} \leq 216.6$ MeV), allowing quadratic energy dependence in the geometrical parameters (a_r, a_i, r_r, r_i), energy independence in the well depths (V_r, V_i), and equal real and imaginary radii. The resulting parameters were first extrapolated to 312.6 MeV and were then used as initial values in a least-squares fit to the elastic scattering data at 312.6 MeV, producing a final χ^2 per point of 0.8 obtained for 5% error bars. The optical potential $I3$, on the other hand, was obtained¹ by individual three-parameter fits to the low-energy data at each energy, requiring that the real and imaginary diffusivities are equal, and leaving V_r and V_i fixed at 50 MeV. The corresponding parameters for the potential $I3$ at 312.6 MeV were derived in a similar manner by a three-parameter ($r_r, r_i, a_r = a_i$) fit to these data, and a final χ^2 per point of 0.06 was obtained. Finally, the optical potential C was obtained¹ from a four-parameter, energy-independent fit to the elastic scattering data be-

tween 104 and 216.6 MeV, requiring that $V_r = 100$ MeV and $V_i = 20$ MeV, and allowing the geometrical parameters (r_r, r_i, a_r, a_i) to vary. The resulting optical-model parameters account reasonably well for the elastic scattering data at 312.6 MeV but, as discussed in Ref. 1, this (or any other) energy-independent potential does not fit the lower energy data as well as do the energy-dependent potentials and, indeed, certain gross discrepancies are found (for example, a complete failure to fit the elastic scattering angular distribution at 216.6 MeV). The parameters for optical potentials Q , $I3$, and C at 312.6 MeV are presented in Table I and the fits to the 312.6 MeV elastic scattering data are displayed in Fig. 7.

A conventional definition²⁴ of the strong absorption radius is the distance of closest approach for a Rutherford trajectory with scattering angle $\theta_{1/4}$, the center-of-mass angle at which the experimental elastic scattering cross section equals $\frac{1}{4}$ of the Rutherford value. This strong absorption radius $R_{1/4}$ is then given by

$$R_{1/4} = \frac{\eta}{k} \left[1 + \csc\left(\frac{1}{2}\theta_{1/4}\right) \right], \quad (5)$$

where $k = (2mE)^{1/2}/\hbar$ is the entrance channel wave number and $\eta = Z_1 Z_2 e^2 \sqrt{m} / \hbar \sqrt{2E}$ is the Sommerfeld parameter. An alternative strong absorption radius can be defined from the grazing angular momentum $l_{1/2}$, for which the optical-potential transmission coefficient T_l equals $\frac{1}{2}$; the distance of closest approach in the corresponding Rutherford trajectory is

$$R_{1/2} = \frac{\eta}{k} \left[1 + \left(1 + \frac{l_{1/2}(l_{1/2}+1)}{\eta^2} \right)^{1/2} \right]. \quad (6)$$

As is discussed in Ref. 25, these two radii are approximately equal in the sharp cutoff limit.

The two strong absorption radii are listed in Table II and displayed in Fig. 8 for the present elastic scattering data and for data^{1,26-28} at incident energies between 80 and 216.6 MeV. Optical potential $I3$ was used for calculations of $l_{1/2}$. The indicated error bars were calculated assuming uncertainties of ± 0.5 and $\pm 0.2^\circ$ in the values of $l_{1/2}$ and $\theta_{1/4}$.

It has recently been noted^{26,29} that for the system $^{16}\text{O} + ^{208}\text{Pb}$ at intermediate incident energies (less than 216.6 MeV), the value of $R_{1/4}$ remains nearly

TABLE I. Optical-potential parameters.

| Potential | V_r (MeV) | V_i (MeV) | r_r (fm) | r_i (fm) | a_r (fm) | a_i (fm) | r_C (fm) |
|-----------|----------------|----------------|---------------|---------------|---------------|---------------|---------------|
| Q | 51.09 | 51.46 | 1.114 | 1.114 | 0.7964 | 0.7410 | 1.300 |
| $I3$ | 50.00 | 50.00 | 1.181 | 1.145 | 0.6820 | 0.6820 | 1.300 |
| C | 100.00 | 20.00 | 1.090 | 1.273 | 0.7770 | 0.5970 | 1.300 |

TABLE II. Interaction radii for $^{16}\text{O} + ^{208}\text{Pb}$ elastic scattering.

| E_{lab} (MeV) | $V_r = V_i$ (MeV) | r_r (fm) | r_i (fm) | $a_r = a_i$ (fm) | $\theta_{1/4}$ (deg) | $l_{1/2}$ | $R_{1/4}$ (fm) | $R_{1/2}$ (fm) |
|---------------------------|----------------------|---------------|---------------|---------------------|-------------------------|-----------|-------------------|-------------------|
| 80.0 ^a | 50.0 | 1.394 | 1.364 | 0.261 | ... | 11.0 | ... | 12.91 |
| 83.0 ^a | 50.0 | 1.406 | 1.351 | 0.243 | 139.0 | 21.7 | 12.67 | 12.95 |
| 88.0 ^a | 50.0 | 1.384 | 1.300 | 0.278 | 114.3 | 30.6 | 12.66 | 12.86 |
| 90.0 ^a | 50.0 | 1.335 | 1.308 | 0.383 | 107.2 | 34.1 | 12.67 | 12.87 |
| 94.0 ^b | 50.0 | 1.295 | 1.283 | 0.460 | 96.2 | 40.0 | 12.68 | 12.88 |
| 96.0 ^a | 50.0 | 1.326 | 1.292 | 0.406 | 91.7 | 42.0 | 12.68 | 12.82 |
| 102.0 ^a | 50.0 | 1.244 | 1.217 | 0.559 | 81.6 | 48.0 | 12.62 | 12.72 |
| 104.0 ^c | 50.0 | 1.317 | 1.293 | 0.419 | 78.1 | 50.9 | 12.65 | 12.79 |
| 129.5 ^d | 50.0 | 1.231 | 1.217 | 0.621 | 52.9 | 73.1 | 12.75 | 12.81 |
| 138.5 ^c | 50.0 | 1.221 | 1.194 | 0.612 | 48.7 | 76.8 | 12.58 | 12.55 |
| 192.0 ^d | 50.0 | 1.215 | 1.198 | 0.625 | 31.2 | 105.8 | 12.50 | 12.46 |
| 216.6 ^c | 50.0 | 1.133 | 1.135 | 0.736 | 27.5 | 115.0 | 12.23 | 12.29 |
| 312.6 | 50.0 | 1.181 | 1.145 | 0.682 | 17.9 | 146.7 | 12.09 | 12.00 |

^aData from Ref. 26.^bData from Ref. 27.^cData from Ref. 1.^dData from Ref. 28.

constant as a function of energy, whereas $R_{1/2}$ appears to decrease slowly as the bombarding energy is increased. With the addition of these new, higher-energy data, it now appears that both radii show a systematic decrease for increasing incident energy, although the magnitude of this effect is rather small. This observation of a decreasing interaction radius is in agreement with the commonly held notion that as the kinetic energy

of the incident particle is increased, the effective interaction region can correspond to smaller radii, and thus, one can sample the field more deeply inside the target nucleus. Additional experimental studies at still higher incident energies and for other nuclear systems (e.g., the $^{16}\text{O} + ^{28}\text{Si}$ system, for which a similarly small effect has been observed³⁰) are clearly necessary for a further investigation and verification of the observed energy dependence of the strong interaction radius.

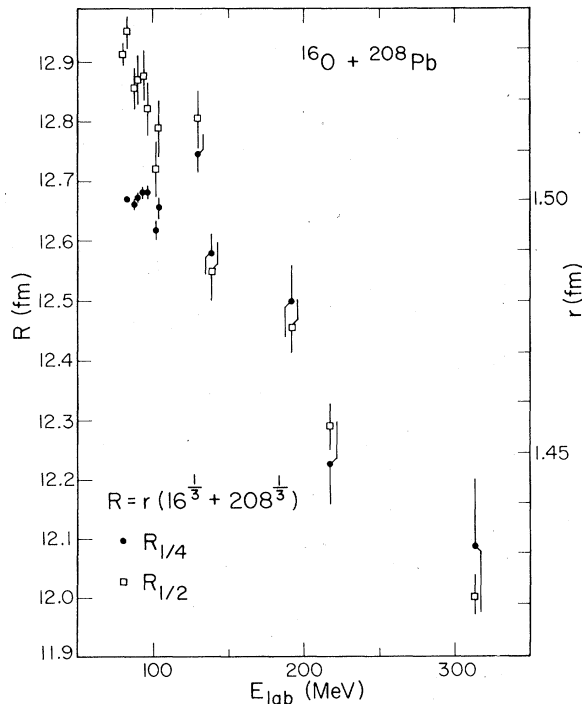


FIG. 8. The strong absorption radii $R_{1/4}$ and $R_{1/2}$ (determined with optical potential I3) as a function of incident energy.

V. SINGLE-NUCLEON TRANSFER ANGULAR DISTRIBUTIONS AND DWBA ANALYSES

A. DWBA calculations

Angular distributions for the $^{208}\text{Pb}(^{16}\text{O}, ^{15}\text{N})^{209}\text{Bi}$ and $^{208}\text{Pb}(^{16}\text{O}, ^{15}\text{O})^{209}\text{Pb}$ reactions at 312.6 MeV were extracted from the data.²² For transitions which were incompletely resolved [such as the $f_{5/2} + p_{3/2} + p_{1/2}$ triplet and $f_{7/2} + i_{13/2}$ doublet observed in the $^{208}\text{Pb}(^{16}\text{O}, ^{15}\text{N})^{209}\text{Bi}$ spectra], yields to the individual states were obtained using a peak-fitting procedure. Yields for the $^{15}\text{N}^*$ and $^{15}\text{O}^*$ transitions were obtained using linear background subtraction techniques; no background was apparent for transitions to the low-lying states in ^{209}Bi and ^{209}Pb . As at the other incident energies above the Coulomb barrier, structureless bell-shaped angular distributions are observed and, in the present work, are peaked at an angle of 13.5° (c.m.). Finite-range DWBA calculations for each of these transitions at all measured energies were made with the program PTOLEMY.²³ The effective transition operator included both Coulomb and core-Coulomb corrections,³¹ which resulted in calculations using post and prior forms of the interaction agreeing with 3%.

The optical-potential parameters which were

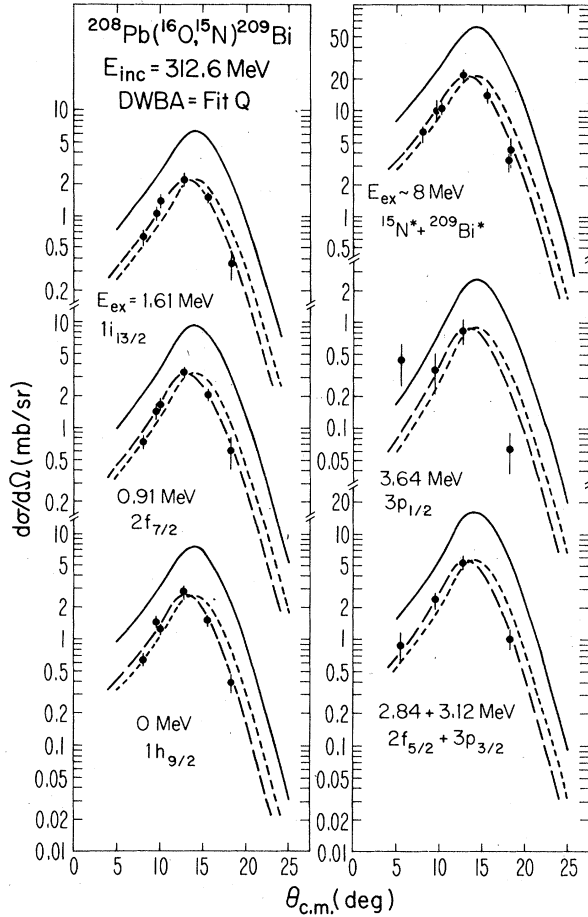


FIG. 9. Angular distributions of the $^{208}\text{Pb}(^{16}\text{O}, ^{15}\text{N})\text{-}^{209}\text{Bi}$ reaction at 312.6 MeV. The solid lines represent DWBA calculations using optical-model potential Q and experimental spectroscopic factors. The short dashed lines indicate the DWBA predictions when the DWBA ground-state angular distribution is normalized to the experimental result; better agreement with the data is obtained when the predictions are shifted by 1° , as indicated by the long dashed lines.

used in the DWBA calculations are presented in Table I and were discussed in Sec. IV. Since detailed $^{15}\text{N} + ^{209}\text{Bi}$ elastic scattering data over a wide range of incident energies are not available (and the short lifetime of ^{15}O prohibits its use as a projectile), identical optical-potential parameters were used in both the entrance and exit channels. The calculations of Ref. 32 indicate that for the $^{208}\text{Pb}(^{12}\text{C}, ^{13}\text{C})^{207}\text{Pb}$ and $^{208}\text{Pb}(^{12}\text{C}, ^{11}\text{B})\text{-}^{209}\text{Bi}$ reactions, DWBA calculations employing optical-model potentials separately determined for both entrance and exit channels were not significantly different from those using the entrance channel optical-model parameters in both channels.

The bound-state wave functions of the transferred

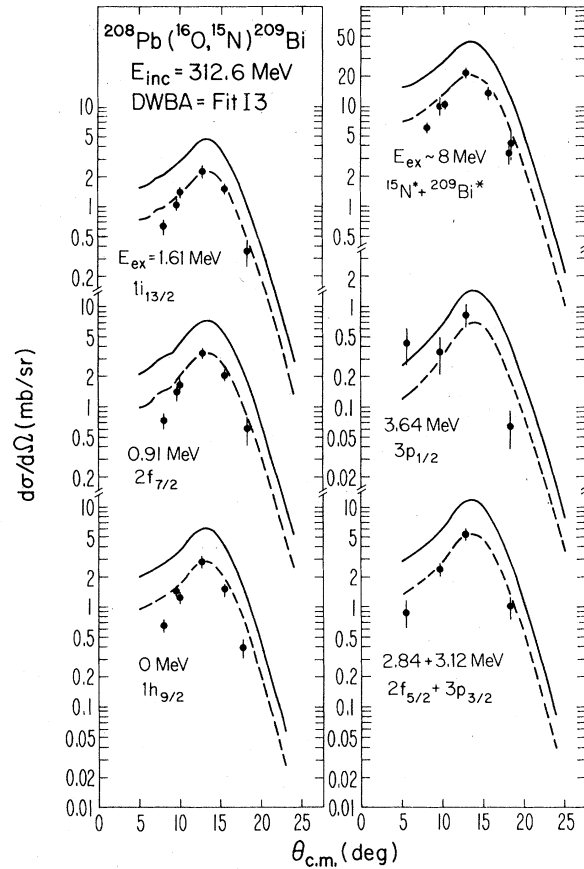


FIG. 10. Angular distributions of the $^{208}\text{Pb}(^{16}\text{O}, ^{15}\text{N})\text{-}^{209}\text{Bi}$ reaction at 312.6 MeV. The solid lines represent DWBA calculations using optical-model potential $I3$ and experimental spectroscopic factors. The dashed lines indicate the DWBA predictions when the DWBA ground-state angular distribution is normalized to the experimental result.

proton and neutron were described by Woods-Saxon potentials, including a spin-orbit interaction. The well depths were adjusted to reproduce the experimental separation energies. The parameters used in the DWBA calculations are listed in Table III and have been used in earlier studies³²⁻³⁴ of heavy-ion induced single-nucleon transfer reactions on ^{208}Pb . A detailed justification of these parameters is given in the previous paper.¹ As was discussed there, the absolute magnitude of the calculated DWBA cross sections is rather sensitive to the choice of bound-state parameters. For example, using the $^{208}\text{Pb} + p$ bound-state potential for the $^{208}\text{Pb} + n$ system increases the calculated $^{208}\text{Pb}(^{16}\text{O}, ^{15}\text{O})^{209}\text{Pb}$ cross sections at 312.6 MeV by a factor of 1.49, but has a similar effect at 139 MeV (the factor is 1.58). As a result, the relative energy dependence of the predicted transfer cross sections will be less sensitive to

TABLE III. Bound-state wave function parameters.

| System | r_r (fm) | a_r (fm) | V_{so} (MeV) | r_{so} (fm) | a_{so} (fm) | r_C (fm) |
|---------------------|---------------|---------------|-------------------|------------------|------------------|---------------|
| $^{208}\text{Pb}+p$ | 1.28 | 0.76 | 6 | 1.09 | 0.06 | 1.30 |
| $^{208}\text{Pb}+n$ | 1.25 | 0.63 | 7 | 1.10 | 0.50 | |
| $^{15}\text{N}+p$ | 1.20 | 0.65 | 7 | 1.20 | 0.65 | 1.20 |
| $^{15}\text{O}+n$ | 1.20 | 0.65 | 7 | 1.20 | 0.65 | |

bound-state parameters.

The spectroscopic factors for ^{15}N and ^{15}O were both assumed to have the full closed-shell value of $S=2$ for the $1p_{1/2}$ ground state and $S=4$ for the excited $1p_{3/2}$ hole state at 6.32 and 6.18 MeV, respectively. The spectroscopic factors for ^{209}Bi and ^{209}Pb given in the last columns of Tables IV and V were taken from vibration-particle coupling calculations^{35,36} which predict strengths roughly consistent with those inferred from earlier studies of light- and heavy-ion induced single-nucleon transfer reactions on ^{208}Pb (see, for example, Refs. 1, 32, 33, 37, and 38). Tables IV and V also list relative spectroscopic factors extracted from the present data using various optical potentials; the absolute ground-state spectroscopic factors are taken from the model calculations of Ref. 35, the light-ion spectroscopic factor S_1 is chosen in the manner described above, and the absolute normalization N is determined from the equation

$$\left(\frac{d\sigma}{d\Omega}\right)_{\text{expt}} = NS_1S_2 \left(\frac{d\sigma}{d\Omega}\right)_{\text{PTOLEMY}} \quad (7)$$

B. $^{208}\text{Pb}(^{16}\text{O}, ^{15}\text{N})^{209}\text{Bi}$ reaction

DWBA calculations for the $^{208}\text{Pb}(^{16}\text{O}, ^{15}\text{N})^{209}\text{Bi}$ reaction at 312.6 MeV are indicated by the solid

lines in Fig. 9 and were obtained using optical potential Q and the experimentally determined relative spectroscopic factors listed in Table IV. The short dashed lines indicate the resulting predictions when the calculated ground-state angular distribution is arbitrarily normalized to the experimental angular distribution, yielding a value of the normalization coefficient $N=0.348$ [see Eq. (7)]. As may be seen, the DWBA generally predicts the shape and position of the angular distributions correctly although, as indicated by the long dashed lines, a somewhat better fit to the data can be obtained by a 1° shift of the DWBA calculations toward smaller scattering angles. It will be demonstrated later that this discrepancy depends on the optical potential used in the calculations.

The generally good agreement of the experimental relative spectroscopic factors with the theoretical values as well as with those measured in earlier studies of single-nucleon transfer reactions on ^{208}Pb indicates that the DWBA accounts reasonably well for the relative intensities of the various transitions and, therefore, for the observed reversal of the j dependence discussed in Sec. III. In addition, DWBA calculations have been performed for the broad structure located at 8 MeV in excitation, assuming this structure to result from the simultaneous excitation of the $1p_{3/2}$ hole state in ^{15}N ($E_{\text{ex}} = 6.32$ MeV, $S=4$) and the six low-lying levels in ^{209}Bi . Using the experimental spectroscopic factors listed in Table IV, and the same normalization factor ($N=0.348$) that was used for transitions involving the ground state of ^{15}N , predictions are obtained that agree quite well with the experimental angular distribution (see Fig. 9). This agreement provides further evidence for the validity of our identification of this structure as due to transfers populating the $p_{3/2}$ hole state of ^{15}N .

TABLE IV. Spectroscopic factors for the $^{208}\text{Pb}(^{16}\text{O}, ^{15}\text{N})^{209}\text{Bi}$ reaction.

| State | E_{ex} (MeV) | Fit Q S^e | Fit $I3$ S^e | $(^{16}\text{O}, ^{15}\text{N})^a$ S^e | $(^{12}\text{C}, ^{11}\text{B})^b$ S | $(^3\text{He}, d)^c$ S | Theory ^d S |
|-------------|--------------------------|-------------------|-------------------|---|---|-----------------------------|----------------------------|
| $1h_{9/2}$ | 0.00 | 0.95 | 0.95 | 0.95 | 0.84 | 1.17 | 0.95 |
| $2f_{7/2}$ | 0.90 | 0.81 | 0.82 | 0.74 | 0.81 | 0.78 | 0.85 |
| $1i_{13/2}$ | 1.61 | 0.73 | 0.68 | 0.61 | 0.75 | 0.56 | 0.70 |
| $2f_{5/2}$ | 2.84 | 0.72 ^f | 0.64 ^f | 0.61 | 0.54 | 0.88 | 0.66 |
| $3p_{3/2}$ | 3.12 | 0.74 ^f | 0.74 ^f | 0.55 | 0.69 | 0.67 | 0.74 |
| $3p_{1/2}$ | 3.64 | 0.66 | 0.50 | 0.52 | ... | 0.45 | 0.54 |

^a From Ref. 1.

^b From Ref. 32, $E_{\text{inc}} = 97.9$ MeV.

^c From Ref. 37.

^d From Ref. 35.

^e Normalized to the theoretical ground-state spectroscopic factor.

^f Spectroscopic factor for the $2f_{5/2}$ level has been adjusted for a small contribution from the unresolved $3p_{3/2}$ level ($S=0.74$ assumed).

TABLE V. Spectroscopic factors for the $^{208}\text{Pb}(^{16}\text{O}, ^{15}\text{O})^{209}\text{Pb}$ reaction.

| State | E_{ex} (MeV) | $E_{inc} = 312.6$ MeV | | 139 MeV ^a | | $(d,p)^b$ S | Theory ^c S |
|---------------|-------------------|-------------------------|--------------------------|-------------------------|--------------------------|----------------|--------------------------|
| | | Fit Q S ^d | Fit I3 S ^d | Fit Q S ^d | Fit I3 S ^d | | |
| $2g_{9/2}$ | 0.00 | 0.89 | 0.89 | 0.89 | 0.89 | 0.92 | 0.89 |
| $1i_{11/2}$ | 0.78 | 0.88 | 0.89 | 0.83 | 0.81 | 1.14 | 0.96 |
| $1j_{15/2}$ | 1.424 | 0.88 ^e | 0.84 ^e | 0.75 ^e | 0.72 ^e | 0.77 | 0.65 ^f |
| $3d_{5/2}$ | 1.565 | 0.91 ^e | 0.91 ^e | 0.91 ^e | 0.91 ^e | 0.89 | 0.91 |
| $4s_{1/2}$ | 2.03 | ... | ... | 9.79 ^g | 6.78 ^g | 0.85 | 0.94 |
| $2g_{7/2}$ | 2.49 | 1.39 ^h | 1.37 ^h | 1.70 ⁱ | 1.81 ⁱ | 0.95 | 0.84 |
| $3d_{3/2}$ | 2.54 | 0.90 ^h | 0.90 ^h | 0.90 ⁱ | 0.90 ⁱ | 0.99 | 0.90 |
| $1j_{15/2}$ | 3.05 | 0.07 ^h | 0.07 ^h | 0.07 | 0.07 | | 0.26 ^f |
| $(1j_{15/2})$ | 3.7 ^j | 0.26 | 0.26 | 0.25 | 0.22 | | |

^aData from Ref. 5 and reanalyzed in the present work.

^bFrom Ref. 38 for an incident energy of 20 MeV.

^cFrom Ref. 35.

^dNormalized to the theoretical ground-state spectroscopic factor.

^eSpectroscopic factor for the $1j_{15/2}$ level has been adjusted for a small contribution from the unresolved $3d_{5/2}$ level ($s = 0.91$ assumed).

^fFrom Ref. 36.

^gApproximate spectroscopic factor (upper limit) since the experimental yields are small and the fits to the data are poor.

^hSpectroscopic factor for the $2g_{7/2}$ level has been adjusted for smaller contributions from the unresolved $3d_{3/2}$ and $1j_{15/2}$ levels ($S = 0.90$ and $S = 0.07$ assumed).

ⁱSpectroscopic factor for the $2g_{7/2}$ level has been adjusted for a small contribution from the unresolved $3d_{3/2}$ level ($S = 0.90$ assumed).

^jApproximate excitation energy. This group could contain transitions to several neighboring states.

The most striking feature shown in Fig. 9 is the failure of the DWBA to predict accurately the absolute magnitude of the transfer cross sections. Although the model properly accounts for the observed relative yields, the DWBA calculations overestimate the magnitude of the cross sections at 312.6 MeV by almost a factor of 3 ($1/N = 2.88$). This effect is also apparent in Fig. 10 where the DWBA angular distributions calculated with optical potential I3 and the corresponding experimental spectroscopic factors (see Table IV) are indicated by the solid lines; the DWBA angular distributions resulting from a normalization of the theoretical and experimental ground-state angular distributions are indicated by the dashed lines. Again, the DWBA overestimates the magnitude of the data by more than a factor of 2 ($1/N = 2.13$). Similar results are also obtained when the energy-independent optical potential C is employed in the DWBA calculations. The shapes of the angular distributions as well as the relative intensities of the various transitions agree reasonably well with the experimental observations. However, the magnitude of the predictions is too large relative to the data by 50% ($1/N = 1.54$).

That the DWBA calculations at 312.6 MeV predict cross sections significantly different from those

observed experimentally is also true at other incident energies. The ground-state angular distributions measured at four incident energies are shown in Fig. 11 (the lower-energy data are from Ref. 1). The solid lines indicate the DWBA cal-

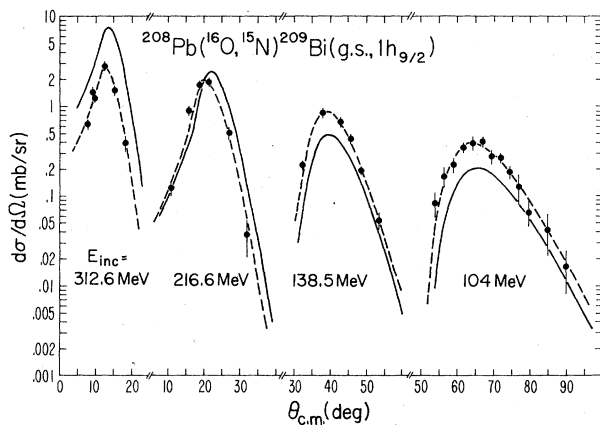


FIG. 11. Angular distributions of the $^{208}\text{Pb}(^{16}\text{O}, ^{15}\text{N})^{209}\text{Bi}$ reaction populating the ground-state of ^{209}Bi at four incident energies. The solid lines represent DWBA calculations using optical-model potential Q and theoretical spectroscopic factors; the dashed lines are the DWBA calculations arbitrarily shifted in magnitude and in angle in order to obtain a best fit to the data.

culations using the optical potential Q with quadratic energy dependence; the dashed lines are drawn to guide the eye. As may be seen, the DWBA predictions reproduce the general shapes of the angular distributions but fail to account for the absolute magnitude of the transfer cross sections as well as the position of the maximum of the angular distributions. At high incident energies, the DWBA predictions overestimate the cross sections, whereas at low incident energies, the predictions significantly underestimate the cross sections.

A more comprehensive comparison of the DWBA results to the data is made in Fig. 12. Here, the energy dependence of the angle-integrated cross sections for each observed transition is shown in the upper part of the figure. The data are indicated by the solid black dots and the corresponding DWBA calculations, using optical potential Q and the theoretical spectroscopic factors (see Table IV) are indicated by the dotted lines. The 69.1 MeV sub-Coulomb transfer data of Ref. 3 and DWBA calculations of Ref. 1 are included in the figure although certain weak transitions were not observed in that work.

At low incident energies, the DWBA reproduces the energy dependence of the angle-integrated transfer cross sections reasonably well, although the actual magnitudes of the cross sections for all transitions are underestimated. At energies above approximately 140 MeV, however, the energy dependence of the experimental cross sections diverges from the DWBA predictions. Whereas the experimental cross sections generally decrease fairly rapidly with incident energy, the predicted cross sections either remain constant in magnitude or increase as the incident energy is increased, resulting in an overestimate of the transfer cross sections at sufficiently high incident energies. These observations are more apparent at the bottom of the figure, where the ratios of the DWBA to experimental cross sections for all observed transitions are shown.

From incident energies below the barrier up to 140 MeV, the ratios of the experimental to theoretical cross sections for the various transitions are almost constant. Above 140 MeV, the ratios increase continuously, indicating that the failure of the DWBA persists up to the highest energy of 312.6 MeV, and is most severe between 140 and 312.6 MeV. The extent to which these conclusions depend upon the particular optical model used in the calculations was investigated by comparing the above results with those of optical potential $I3$ (individual fits at each energy) and with C (energy independent). In Figs. 13(a) and 13(b) are displayed the experimental and theo-

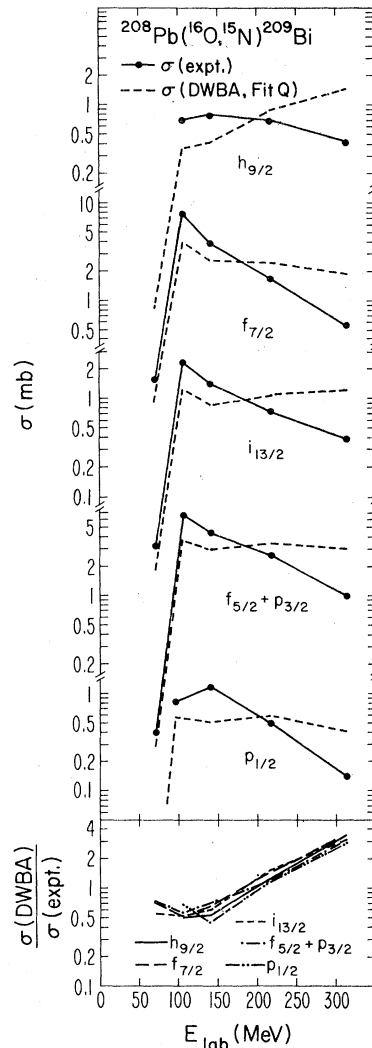


FIG. 12. Experimental and DWBA angle-integrated cross sections for the $^{208}\text{Pb}(^{16}\text{O},^{15}\text{N})^{209}\text{Bi}$ reaction as a function of incident energy using optical-model potential Q and theoretical spectroscopic factors. The ratios of DWBA to experimental cross sections for all measured transitions are shown at the bottom of figure.

retical angle-integrated cross sections, as well as the resulting ratios of experimental and theoretical cross sections, using these optical potentials and the theoretical spectroscopic factors (see Table IV). By comparing these with Fig. 12, it is evident that the DWBA predictions of the energy variation depend to some extent on the optical potentials. However the general trend of constant or increasing theoretical cross sections, compared to decreasing experimental cross sections, persists for all optical potentials at energies above 140 MeV.

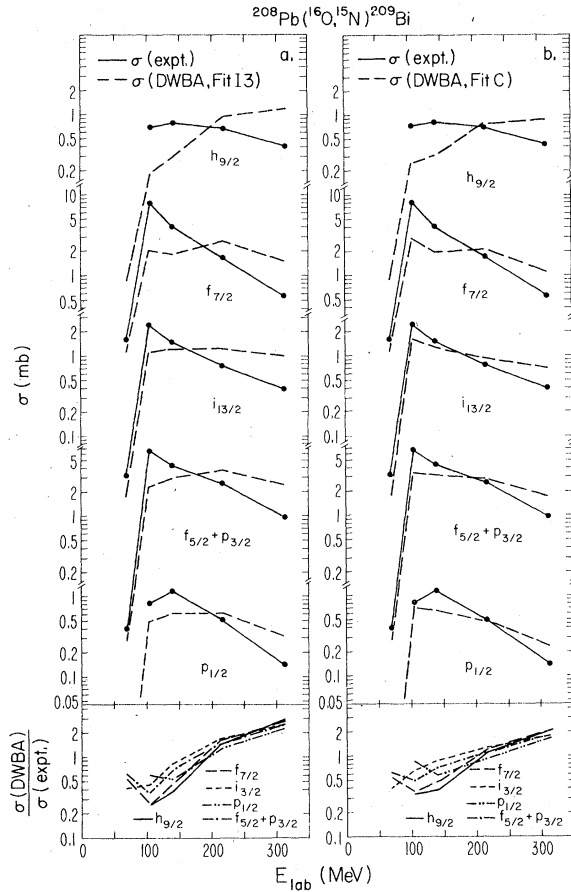


Fig. 13. Experimental and DWBA angle-integrated cross sections for the $^{208}\text{Pb}(^{16}\text{O}, ^{15}\text{N})^{209}\text{Bi}$ reaction as a function of incident energy, using optical-model potentials I3 [part (a)] and C [part (b)] and theoretical spectroscopic factors. The ratios of DWBA to experimental cross sections for all measured transitions are shown at the bottom of the figure.

C. $^{208}\text{Pb}(^{16}\text{O}, ^{15}\text{O})^{209}\text{Pb}$ reaction

The experimental angular distributions for the $^{208}\text{Pb}(^{16}\text{O}, ^{15}\text{O})^{209}\text{Pb}$ reaction are shown in Fig. 14, together with DWBA calculations (solid lines) using optical potential Q and the corresponding experimental spectroscopic factors (see Table V). The dashed lines indicate the resulting DWBA predictions when the experimental and theoretical ground-state angular distributions are normalized, requiring a value of the normalization coefficient $N=0.371$. As with the proton-transfer data, the DWBA accurately predicts the shapes of the angular distributions as well as the relative intensities of the transitions to different single-particle states. Again, DWBA calculations for the broad structure located near 8 MeV in excitation are in agreement with our identification of this structure as the result of transfer to the $p_{3/2}$ hole state in ^{15}O .

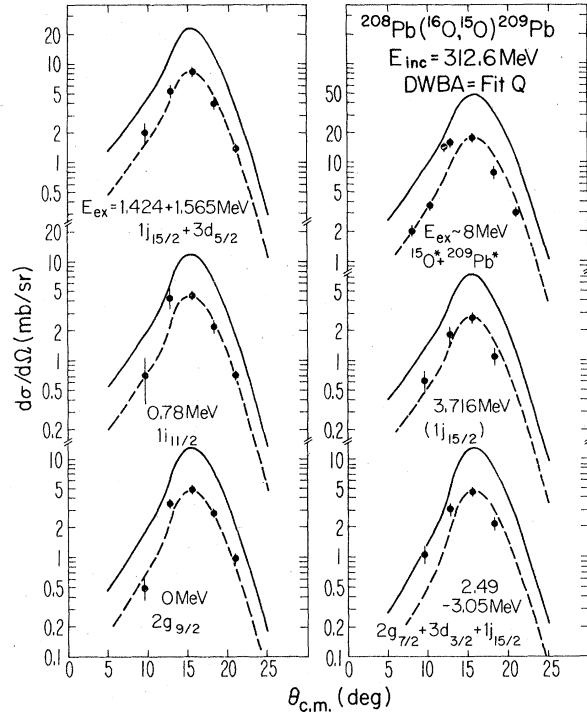


FIG. 14. Angular distributions of the $^{208}\text{Pb}(^{16}\text{O}, ^{15}\text{O})^{209}\text{Pb}$ reaction at 312.6 MeV. The solid lines represent DWBA calculations using optical-model potential Q and experimental spectroscopic factors. The dashed lines indicate the DWBA predictions when the DWBA ground-state angular distribution is normalized to the experimental result.

Our analysis of the possible $1j_{15/2}$ single-particle fragment states in ^{209}Pb is hindered somewhat by an uncertainty in their theoretical spectroscopic factors. Reference 35 presented spectroscopic factors which were averaged over excitation energy. The calculations of Refs. 36 and 39 also indicate substantial $1j_{15/2}$ single-particle strength between 3 and 4 MeV in excitation, but Refs. 36 and 39 differ significantly in the predicted locations and strengths of these fragment states and fail to reproduce the observed single-particle fragmentation measured, for example, in studies³⁸ of the (d, p) reaction on ^{208}Pb . In addition, the fragment strengths observed in the present work may not be completely accurate, since (i) the yields obtained for the transition near 3.72 MeV could contain yields from possible neighboring weak transitions, and (ii) the weak transition to the $j_{15/2}$ state at 3.05 MeV would not be resolved from transitions to other states between 2.5 and 3.5 MeV, in particular a strong transition to the $g_{7/2}$ level at 2.49 MeV. As a result of these problems, neither the experimental nor the theoretical spectroscopic factors quoted in Table V for the two fragment states are very reliable, but they still indicate

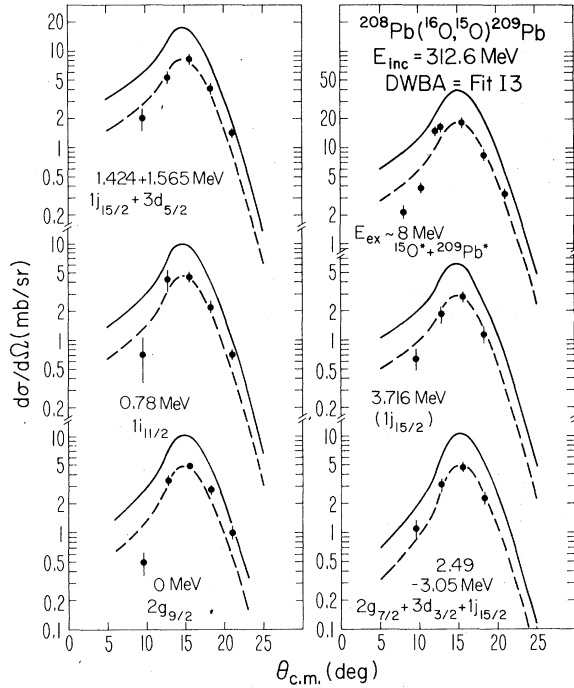


FIG. 15. Angular distributions of the $^{208}\text{Pb}(^{16}\text{O}, ^{15}\text{O})\text{-}^{209}\text{Pb}$ reaction at 312.6 MeV. The solid lines represent DWBA calculations using optical model potential *I3* and experimental spectroscopic factors. The dashed lines indicate the DWBA predictions when the theoretical ground-state angular distribution is normalized to the experimental result.

that a significant fraction of the $1j_{15/2}$ single-particle strength is fragmented and located between 3 and 4 MeV in excitation.

As was found for the proton-transfer reaction, the DWBA predictions for the neutron-transfer cross sections at 312.6 MeV significantly exceed the experimental values. This effect does not depend on the particular optical potential used in the calculations, as may be observed by comparing Figs. 14 and 15, in which the DWBA calculations performed using optical potentials *Q* and *I3* respectively are shown; the corresponding experimental spectroscopic factors are listed in Table V.

The $^{208}\text{Pb}(^{16}\text{O}, ^{15}\text{O})\text{-}^{209}\text{Pb}$ reaction has not been studied as extensively as the $^{208}\text{Pb}(^{16}\text{O}, ^{15}\text{N})\text{-}^{209}\text{Bi}$ reaction, and data are available at only one other incident energy.⁵ In order to compare these data in a consistent manner, the data at 139 MeV⁵ have been reanalyzed following the methods discussed in Sec. VA and using the $^{16}\text{O} + ^{208}\text{Pb}$ optical potentials employed in the proton-transfer analyses. The resulting angular distributions are displayed in Figs. 16 and 17 for optical potentials *Q* and *I3*, respectively, and using the experimental spectroscopic factors given in Table V. These

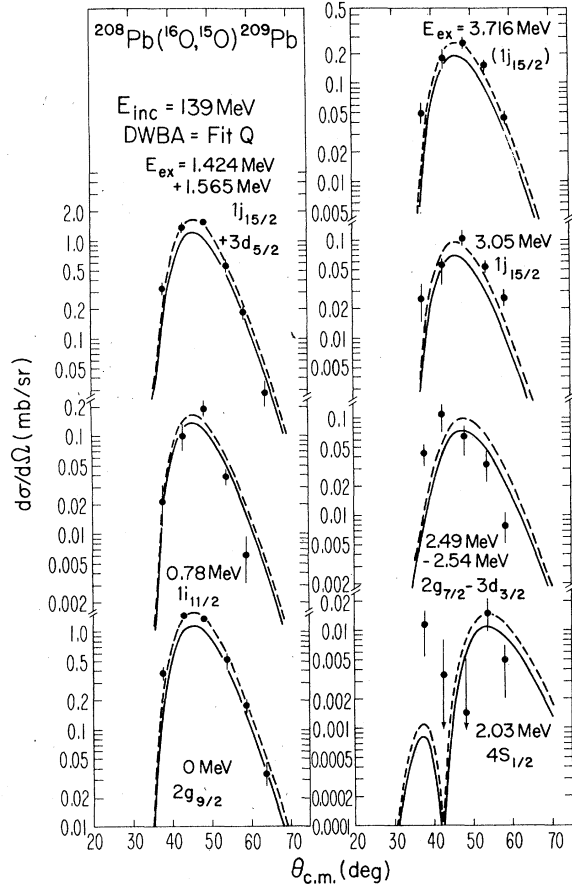


FIG. 16. Angular distributions of the $^{208}\text{Pb}(^{16}\text{O}, ^{15}\text{O})\text{-}^{209}\text{Pb}$ reaction at 139 MeV. The solid lines represent DWBA calculations using optical-model potential *Q*. The dashed lines indicate the DWBA predictions when the theoretical ground-state angular distribution is normalized to the experimental result.

spectroscopic factors are generally in good agreement with those obtained in Ref. 5. Here, however, somewhat different shapes of the angular distributions are calculated and the angular shift of the calculations relative to the data which was observed in Ref. 5 does not appear for a number of the states in the present calculations. An additional difference between the DWBA calculations presented here and in Ref. 5 is the quite different shape of the angular distribution calculated for the $4s_{1/2}$ transition. The secondary maximum in the angular distribution located at 37° is an order of magnitude smaller in the present calculations than in Ref. 5. This difference reflects the special convergence problems encountered in calculations of the poorly matched $4s_{1/2}$ transition. The 1–2% accuracy achieved for the $4s_{1/2}$ calculations shown in Figs. 16 and 17 requires a very large number of integration points—

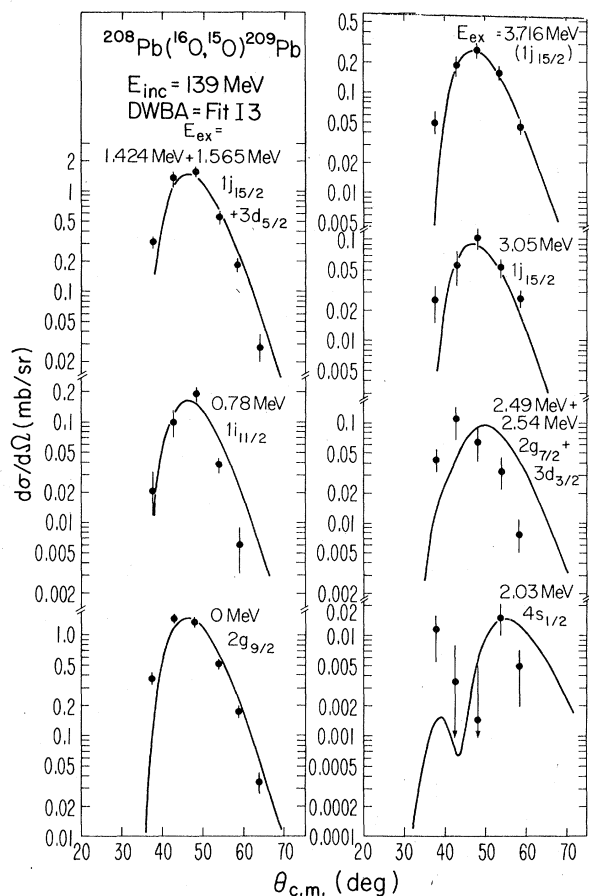


FIG. 17. Angular distributions of the $^{208}\text{Pb}(^{16}\text{O}, ^{15}\text{O})\text{-}^{209}\text{Pb}$ reaction at 139 MeV. The solid lines represent DWBA calculations using optical model potential I3.

many more than were practical using the programs available when Ref. 5 was published.

The experimental angle-integrated cross sections for the $^{209}\text{Pb}(^{16}\text{O}, ^{15}\text{O})^{209}\text{Pb}$ reaction at 139 and 312.6 MeV are displayed in Figs. 18 (a) and 18(b). These figures also show the calculated total transfer cross sections using optical potentials Q and I3, respectively, and the theoretical spectroscopic factors listed in Table V. (Since, as discussed earlier, the theoretical spectroscopic factor for the possible $1j_{15/2}$ fragment state at 3.72 MeV is extremely uncertain, the energy-averaged experimental spectroscopic factor for each optical potential was used for display purposes.) As may be seen, there is a general tendency of the DWBA calculations to increase with incident energy more rapidly than the data. This effect is similar to what was observed in analyses of the proton-transfer data, although the severity of this discrepancy appears to be less for the neutron-transfer reaction.

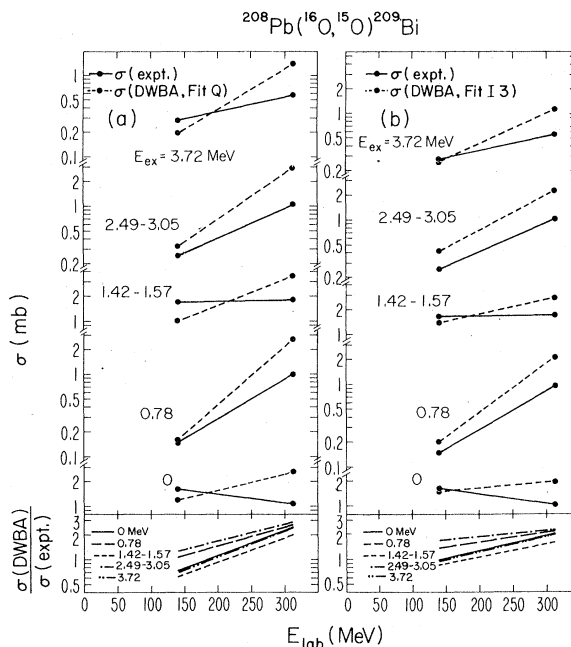


FIG. 18. Experimental and DWBA angle-integrated cross sections for the $^{208}\text{Pb}(^{16}\text{O}, ^{15}\text{O})^{209}\text{Pb}$ reaction as a function of incident energy using optical-model potentials Q (part a) and I3 (part b) and theoretical spectroscopic factors. The ratios of DWBA to experimental cross sections for all measured transitions are shown at the bottom of the figure.

D. Discussion

It has been demonstrated that the energy dependence of the transfer cross sections predicted by the DWBA disagrees with experiment. A similar discrepancy is encountered in DWBA analyses¹ of the $^{208}\text{Pb}(^{16}\text{O}, ^{17}\text{O})^{207}\text{Pb}$ reaction at lower incident energies. It should be noted once again that the overall absolute normalization of the DWBA calculations is not well determined and can be varied in an energy-independent way, for example, by adjustments of the bound-state parameters. However, such adjustments have similar effects at all energies so that the discrepancy in the energy dependence is not removed. One consequence of this observation is that the precise energy at which the experimental and DWBA cross sections are equal is not physically significant since it depends on the absolute normalization of the DWBA cross sections. The important observation is that the ratios of the theoretical to experimental cross sections do not remain constant with energy, and the variation appears to be most severe at energies above 140 MeV.

As discussed in the previous paper,¹ the DWBA cross sections are sensitive to only the asymptotic regions of the bound-state wave functions,

where the shape of the wave function is determined by the particle separation energy. Consequently, as was demonstrated earlier, reasonable changes in the bound-state parameters do not change the energy dependence of the DWBA predictions.

Adjustment of the optical-potential parameters does have some influence on the absolute normalization of the DWBA as well as on the specific details of the predicted energy dependence, as can be seen by comparing the energy dependence of the cross section ratios in Figs. 12, 13 (a), and 13 (b). The important point to note, however, is that no reasonable adjustment of the model parameters can bring the energy dependence of the DWBA cross sections into agreement with experiment. Of course, agreement between the DWBA and experimental cross sections at the various incident energies could be obtained by *ad hoc* variations at each energy of the bound-state and optical-potential parameters, sacrificing, if necessary, both the qualitative relationship of the bound-state potentials to the nucleon-nucleus optical model as well as the quality of optical-model fits to the elastic scattering data. Such modifications, however, completely ignore the basic premises of the DWBA optical-model treatment of direct reactions and, moreover, have no predictive power.

Earlier DWBA analyses (e.g., Refs. 4, 32) of low-energy ^{16}O - and ^{12}C -induced one-proton transfer reactions on ^{208}Pb have revealed an additional failure of the DWBA, namely, that the DWBA predicts angular distributions which are shifted in angle relative to the data. The failure does not appear to result from the particular optical potential employed in the DWBA calculations, providing the optical potential gives a good representation of the elastic data. This effect is illustrated in Fig. 11 for the $(^{16}\text{O}, ^{15}\text{N})$ reaction populating the ground state of ^{209}Bi at four incident energies. As can be seen, this peak angle shift is most prominent at lower incident energies and does not appear to be present at 312.6 MeV, although a peak angle shift of less than 1° would also be consistent with the data.

Recent theoretical efforts⁴⁰ have suggested that significant differences between the DWBA predictions and experimental observations, such as the peak angle shift, could result from a large polarization of the single-particle wave functions during the collision. (An extreme limit of this effect would be adiabatic two-center shell-model wave functions.) Inclusion of this effect in the model calculations might significantly change both the absolute cross sections and the peak angle, but it is expected to be important mainly at low incident energies (near the Coulomb barrier) where

the orbitals have sufficient time to rearrange themselves, i.e., where the transit time is longer than the internal nuclear relaxation time. However, at low incident energies, the failure of the DWBA energy dependence, if indeed present, is generally less severe than at high incident energies. In addition, polarization effects are predicted to be most important for the most weakly bound states, whereas the failure of the DWBA energy dependence appears to be comparable for all final states. As a result of these two observations, polarization effects are not expected to account for the failure of the DWBA energy dependence over the entire range of incident energies.

An alternative explanation of this failure is suggested by the energy spectra for the ^{208}Pb - $(^{16}\text{O}, ^{15}\text{N})^{209}\text{Bi}$ reaction shown in Fig. 1. In addition to the low-lying single-particle transitions, a large yield to the quasielastic continuum is exhibited at 312.6 MeV, centered at about 15 MeV in excitation (see Fig. 3), but is only weakly seen at lower incident energies. It may be possible that the large flux populating states in the continuum at high incident energies is related to the failure of the DWBA energy dependence, which also is most severe at the highest incident energies. Such an explanation would also account rather well for the neutron-transfer data for which the continuum cross section is not as enhanced and the DWBA failure not as severe as for the proton-transfer data. These considerations are currently under investigation,⁴¹ and a multistep direct reaction approach (i.e., coupled channels calculations) is being employed in an attempt to reproduce the continuum energy spectra usually observed in transfer reactions. If this model is successful and, in particular, if it can account for the increased yield to the continuum for higher incident energies, then a proper description of the energy dependence of transitions to the discrete low-lying states might also result. An investigation of the energy dependence expected for multistep transfer reactions populating discrete low-lying states in the residual nuclei might also be relevant, although it is difficult to imagine how such considerations can account for the energy-dependent, but j -independent effects demonstrated here.

A further possibility is that the failure of the DWBA to reproduce the observed energy dependence of the transfer cross sections may reflect an inadequate treatment of the bound-state contributions to the transfer amplitudes. These enter through matrix elements of an effective interaction operator between single-nucleon form factors at the target and projectile vertices, integrated over the internal coordinates of the cores. The effective interaction used in conven-

tional DWBA or coupled-channel Born-approximation (CCBA) calculations is at best a crude guess; a more fundamental theory in terms of the underlying nucleon-nucleon interactions may yield an effective interaction whose energy dependence is significant. The replacement of the single-nucleon form factor by Woods-Saxon wave functions is also an approximation. However, the form factors necessarily reduce at large R to an exponential form $e^{-\gamma R}$, with γ determined by the binding energy difference between initial and final nuclear states. To better than 10%, the transfer cross sections are sensitive to the form factors only in the region where they have healed to the exponential asymptotic form. The large discrepancy between the DWBA and the experimental energy dependence of the transfer cross sections is unlikely to be corrected by straightforward modifications of the bound-state matrix elements.

VI. CONCLUSIONS

In this and the preceding paper¹ it has been shown that DWBA analyses of the $^{208}\text{Pb}(^{16}\text{O}, ^{15}\text{N})$ - ^{209}Bi and $^{208}\text{Pb}(^{16}\text{O}, ^{15}\text{O})^{209}\text{Pb}$ reactions accurately reproduce the relative yields of the various transitions at each incident energy and consequently can account for the reversal of the j dependence observed in the proton-transfer data. However, the energy dependence of the transfer cross sections predicted by the DWBA is in serious disagreement with the data. Significantly larger cross sections are predicted than observed at the higher incident energies; the discrepancy involves factors of 2 to 3 at 312.6 MeV. This failure of the DWBA is a serious problem and warrants further investigation, since this theory is currently our most widely used model of the transfer process.

Perhaps one of the first questions to be addressed is whether this failure is unique to heavy-ion transfer reactions or is also present for light-ion transfer reactions. In a recent study, it was concluded that no systematic energy variation in the ratio $\sigma(\text{DWBA})/\sigma(\text{expt})$ was indicated for the reaction $^{58}\text{Ni}(^3\text{He}, \alpha)^{57}\text{Ni}$ from 15 to 205 MeV, as shown by the solid line in Fig. 19. However, this conclusion relies heavily on the data at 205 MeV, for which no elastic scattering data were obtained and for which the optical potential used in the calculations was an unverified linear extrapolation from data below 83.5 MeV. The dashed line in Fig. 19 is the result of a least-squares fit to the ratios of the cross sections, omitting the data at 205 MeV. The elimination of this point results in

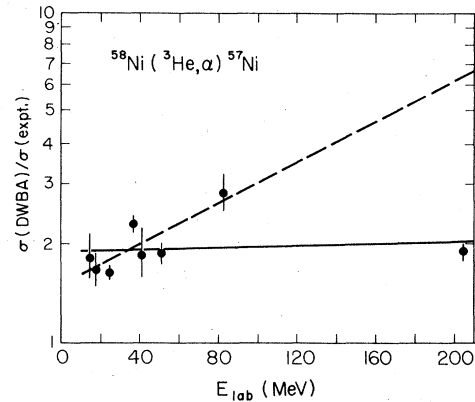


FIG. 19. Ratios of DWBA to experimental cross sections for the $^{58}\text{Ni}(^3\text{He}, \alpha)^{57}\text{Ni}$ reaction. (See Ref. 42 for a discussion of the DWBA calculations.)

a plot that indicates an increase in $\sigma(\text{DWBA})/\sigma(\text{expt})$ by a factor of 2 between 15 and 83.5 MeV. This effect is qualitatively similar to, although smaller than, the effect noted in the present work. In addition, preliminary analyses⁴³ of high-energy (p, d) transfer reactions on medium and heavy nuclei indicate that for an incident energy of 121.2 MeV, the DWBA predictions are significantly larger than the observed transfer cross sections. Such studies, in conjunction with heavy-ion transfer studies, are crucial for an ultimate understanding of this failure of the DWBA.

The importance of studying reactions over a wide range of incident energies has been demonstrated. Our study reveals a serious shortcoming of the DWBA that would not have been evident in reaction studies at a single or a few closely spaced energies. Systematic studies of elastic scattering and transfer reactions from below the Coulomb barrier to as high above the barrier as is experimentally feasible are clearly useful and necessary for a complete investigation of the mechanism of transfer reactions.

ACKNOWLEDGMENTS

The authors are pleased to acknowledge A. Menchaca-Rocha for participation in the early experiments, J. Bowen, D.J. Clark, R.A. Gough, W. Holley, and the accelerator crew for the excellent quality, high-intensity $^{16}\text{O}^{6+}$ beams, C. Ellsworth for preparation of the ^{208}Pb targets, and the personnel of the 88-inch cyclotron for their support and assistance throughout these studies. This work was performed under the auspices of the U.S. Department of Energy.

- *Present address: Physics Division, Argonne National Laboratory, Argonne, Illinois 60439.
- †Permanent address: Centre d'Etudes Nucléaires de Saclay, Gif-sur-Yvette 91190, France.
- ‡Permanent address: Institut des Sciences Nucléaires, Grenoble, France.
- §Present address: Department of Physics, Michigan State University, East Lansing, Michigan 48824.
- ¹S. C. Pieper, M. H. Macfarlane, D. H. Gloeckner, D. G. Kovar, F. D. Becchetti, B. G. Harvey, D. L. Hendrie, H. Homeyer, J. Mahoney, F. Pühlhofer, W. von Oertzen, and M. S. Zisman, preceding paper. *Phys. Rev. C* **18**, 180 (1978).
 - ²C. Olmer, M. C. Mermaz, M. Buenerd, C. K. Gelbke, D. L. Hendrie, J. Mahoney, A. Menchaca-Rocha, D. K. Scott, M. H. Macfarlane, and S. C. Pieper, *Phys. Rev. Lett.* **38**, 476 (1977).
 - ³A. R. Barnett, W. R. Phillips, P. J. A. Buttle, and L. J. B. Goldfarb, *Nucl. Phys.* **176**, 321 (1971).
 - ⁴D. G. Kovar, B. G. Harvey, F. D. Becchetti, J. Mahoney, D. L. Hendrie, H. Homeyer, W. von Oertzen, and M. A. Nagarajan, *Phys. Rev. Lett.* **30**, 1075 (1973).
 - ⁵F. D. Becchetti, B. G. Harvey, D. Kovar, J. Mahoney, C. Maguire, and D. K. Scott, *Phys. Rev. C* **12**, 894 (1975).
 - ⁶M. Buenerd, C. K. Gelbke, B. G. Harvey, D. L. Hendrie, J. Mahoney, A. Menchaca-Rocha, C. Olmer, and D. K. Scott, *Phys. Lett.* **37**, 1191 (1976).
 - ⁷C. K. Gelbke, M. Buenerd, D. L. Hendrie, J. Mahoney, M. C. Mermaz, C. Olmer, and D. K. Scott, *Phys. Lett.* **65B**, 227 (1976).
 - ⁸C. K. Gelbke, D. K. Scott, C. Olmer, M. Buenerd, D. L. Hendrie, J. Mahoney, and M. C. Mermaz (unpublished).
 - ⁹B. G. Harvey, J. Mahoney, F. G. Pühlhofer, F. S. Goulding, D. A. Landis, J. C. Faivre, D. G. Kovar, M. S. Zisman, J. R. Meriwether, S. W. Cosper, and D. L. Hendrie, *Nucl. Instrum. Methods* **104**, 21 (1972).
 - ¹⁰H. Homeyer, J. Mahoney, and B. G. Harvey, *Nucl. Instrum. Methods* **118**, 311 (1974).
 - ¹¹B. G. Harvey, J. Mahoney, and R. F. Burton, Annual Report, Nuclear Science Division, Lawrence Berkeley Laboratory, 1975, (unpublished) p. 354.
 - ¹²B. G. Harvey, J. Mahoney, and R. F. Burton (unpublished).
 - ¹³D. G. Kovar, F. D. Becchetti, B. G. Harvey, F. Pühlhofer, J. Mahoney, D. W. Miller, and M. S. Zisman, *Phys. Rev. Lett.* **29**, 1023 (1972).
 - ¹⁴D. M. Brink, *Phys. Lett.* **40B**, 37 (1972).
 - ¹⁵N. Anyas-Weiss, J. C. Cornell, P. S. Fisher, P. N. Hudson, A. Menchaca-Rocha, D. J. Millener, A. D. Panagiotou, D. K. Scott, D. Strottman, D. M. Brink, B. Buck, P. J. Ellis, and T. Engeland, *Phys. Lett. C* **12**, 201 (1974).
 - ¹⁶F. E. Bertrand and D. C. Kocher, *Phys. Rev. C* **13**, 2241 (1976).
 - ¹⁷G. R. Satchler, *Phys. Rev. C* **14**, 97 (1974), and references therein.
 - ¹⁸D. H. Youngblood, J. M. Moss, C. M. Rozsa, J. D. Bronson, A. D. Bacher, and D. R. Brown, *Phys. Rev. C* **13**, 994 (1976).
 - ¹⁹M. Sasao and Y. Torizuka, *Phys. Rev. C* **15**, 217 (1977).
 - ²⁰D. Ashery, M. S. Zisman, R. B. Weisenmiller, A. Guterman, D. K. Scott, and C. F. Maguire, Annual Report, Nuclear Science Division, Lawrence Berkeley Laboratory, 1975 (unpublished) p.97.
 - ²¹C. K. Gelbke, C. Olmer, M. Buenerd, D. L. Hendrie, J. Mahoney, M. C. Mermaz, and D. K. Scott, Lawrence Berkeley Laboratory Report No. LBL-5826, 1977 (unpublished).
 - ²²See AIP document number PAPS PRVCA-18-205-4 for tabulations of the data reported in this article. Order by PAPS number and journal reference from American Institute of Physics, Physics Auxiliary Publication Service, 335 East 45th Street, New York, NY 10017. The price is \$1.50 for microfiche or \$5.00 for a photocopy. Make checks payable to AIP. This material also appears in *Current Physics Microfilms* on the frames immediately following this journal article.
 - ²³D. H. Gloeckner, M. H. Macfarlane, and S. C. Pieper, Argonne National Laboratory Report No. ANL-76-11 1976 (unpublished).
 - ²⁴J. S. Blair, *Phys. Rev.* **95**, 1218 (1954).
 - ²⁵W. E. Frahn and R. H. Venter, *Ann. Phys. (N. Y.)* **24**, 243 (1963).
 - ²⁶F. Videbaek, R. B. Goldstein, L. Grodzins, S. G. Steadman, T. A. Belote, and J. D. Garrett, in *Proceeding of the Symposium on Macroscopic Features of Heavy-Ion Collisions* [Argonne National Laboratory Report No. ANL/PHY-76-2, (unpublished)] p. 819.
 - ²⁷J. D. Garrett, A. Z. Schwarzschild, C. E. Thorn, and W. von Oertzen, *Bull. Am. Phys. Soc.* **19**, 1025 (1974).
 - ²⁸J. B. Ball, C. B. Fulmer, E. E. Gross, M. L. Halbert, D. C. Hensley, C. A. Ludemann, M. J. Saltmarsh, and G. R. Satchler, *Nucl. Phys.* **A252**, 208 (1975).
 - ²⁹F. Videbaek, R. B. Goldstein, L. Grodzins, S. G. Steadman, T. A. Belote, and J. D. Garrett, *Phys. Rev. C* **15**, 954 (1977).
 - ³⁰J. G. Cramer and R. M. DeVries (unpublished); J. G. Cramer, *Bull. Am. Phys. Soc.* **21**, 991 (1976).
 - ³¹R. M. DeVries, G. R. Satchler, and J. G. Cramer, *Phys. Rev. Lett.* **32**, 1377 (1974).
 - ³²K. S. Toth, J. L. C. Ford, Jr., G. R. Satchler, E. E. Gross, D. C. Hensley, S. T. Thornton, and T. C. Schweizer, *Phys. Rev. C* **14**, 1471 (1976).
 - ³³K. S. Low and T. Tamura, *Phys. Rev. C* **11**, 789 (1975).
 - ³⁴J. L. C. Ford, Jr., K. S. Toth, G. R. Satchler, D. C. Hensley, L. W. Owen, R. M. DeVries, R. M. Gaedke, P. J. Riley, and S. T. Thornton, *Phys. Rev. C* **10**, 1429 (1974).
 - ³⁵P. Ring and E. Werner, *Nucl. Phys.* **A211**, 198 (1973).
 - ³⁶I. Hamamoto, *Nucl. Phys.* **A126**, 545 (1969); **A141**, 11 (1970).
 - ³⁷C. Ellegaard and P. Vedelsby, *Phys. Lett.* **26B**, 155 (1968).
 - ³⁸D. G. Kovar, N. Stein, and C. K. Bockelman, *Nucl. Phys.* **A231**, 266 (1974); C. F. Maguire, D. G. Kovar, W. D. Callender, and C. K. Bockelman, *Phys. Rev. C* **15**, 170 (1977).
 - ³⁹D. Bes and R. Broglia, *Phys. Rev. C* **3**, 2389 (1971).
 - ⁴⁰K. Pruess, G. Delic, L. A. Charlton, and N. K. Glendenning, in *Proceedings of the Symposium on Macroscopic Features of Heavy-Ion Collisions* [Argonne National Laboratory Report No. ANL/PHY-76-2, (unpublished)] p. 723.
 - ⁴¹T. Udagawa, B. T. Kim, and T. Tamura, *Bull. Am. Phys. Soc.* **22**, 565 (1977).
 - ⁴²J. R. Shepard, W. R. Zimmerman, and J. J. Kraushaar, *Nucl. Phys.* **A275**, 189 (1977).
 - ⁴³J. J. Kraushaar, R. E. Anderson, J. R. Shepard, and J. R. Comfort, *Bull. Am. Phys. Soc.* **22**, 562 (1977).